Magnetic Behavior of NO Fe-Si Sheets Under Tensile and Compressive Stresses

Magnetic Behavior of NO Fe–Si Sheets Under Tensile and Compressive Stresses

Carlo Appino[1], Enzo Ferrara[1], Olivier de la Barrière[2], Daniele Carosi[3] Alessandro Morri[3], Alessandro Ferraiuolo[4], and Fausto Fiorillo[1]

[1]Istituto Nazionale di Ricerca Metrologica (INRIM), 10135 Turin, Italy
[2]Laboratoire SATIE, CNRS/ENS Paris Saclay, 91190 Gif-sur-Yvette, France
[3]Department of Industrial Engineering, Università di Bologna, 40126 Bologna, Italy
[4]Marcegaglia Ravenna S.p.A., 48123 Ravenna, Italy

The stress dependence of the magnetic properties of non-oriented (NO) Fe–Si steel sheets has been investigated by measurement and analysis of hysteresis loop, magnetization curve, and energy losses taken at different peak polarization values J_p (0.5–1.5 T) between dc and $f = 400$ Hz. The salient feature of the material response to the stress lies in the monotonic deterioration of the soft magnetic properties, across the whole ($J_p - f$) domain, on passing from the maximum tensile stress ($\sigma = +30$ MPa) to the maximum compression ($\sigma = -30$ MPa). This is understood in terms of stress-induced redistribution of the domains between easy axes, making magnetic hardening by compression directly related to unfavorably directed domains and 90° domain-wall-mediated magnetization transitions. The loss decomposition is carried out across the whole investigated frequency range, taking into account the skin effect at the highest frequencies. Quasi-static and dynamic losses follow similar behaviors, both monotonically increasing on passing from the tensile to the compressive stress limits, according to the theoretically expected relationship existing between the hysteresis and the excess loss components.

Index Terms— **Loss decomposition, magnetic losses, magnetoelastic properties, mechanical stress, non-oriented (NO) Fe–Si sheets.**

I. Introduction

ELECTRICAL machine cores are always subjected to mechanical stresses, a condition deriving in the first place from punching and assemblage of the steel sheets and made worse in the running machine by magnetostrictive effects, centrifugal forces, and heat shrinking [1], [2], [3]. The magnetoelastic energy content and its unfolding throughout the magnetization process, via the domain structure and the motion of the domain walls (dws), is responsible for the stress sensitivity of the magnetic sheets. Compressive (negative) stress σ is distinctly detrimental to the soft magnetic response of the non-oriented (NO) Fe–Si alloys, the lower the Si content, the stronger the deterioration of permeability and losses [4]. This effect, descending from the positive value of the saturation magnetostriction constant λ_s, is well known and phenomenologically understood [5], [6]. For the same reason, tensile (positive) stress is beneficial to permeability and loss properties, at least up to some 30–50 MPa, beyond which it monotonically increases until yield [7], [8], [9], [10]. The modeling of quasi-static magnetization curve and hysteresis loop and their evolution with the applied stress σ have been for the main part treated in the frame of the Jiles–Atherton model of hysteresis, where a stress field $H_\sigma = (3/2)\sigma(d\lambda/dJ)$, with λ the relative magnetostrictive elongation and J the material polarization, is introduced and added to the applied and demagnetizing fields [11], [12]. The Jiles–Atherton model was combined in [13] with a single-valued free-energy-based magnetic constitutive law to predict stress-dependent coercive field and hysteresis. The presence of a common crossover point occurring on the hysteresis loops under compressive stress in the second and fourth quadrants has also been highlighted [6], [14].

The ac soft magnetic properties, following a similar trend with σ as the quasi-static hysteresis, are generally assessed at power frequencies by invoking the loss decomposition model [7], [8], [9], [15]. The use of Steinmetz's equation [3] has been proposed, as well as the adoption of an equivalent elliptical loop as the magnetic constitutive equation of the material [16]. No treatment of the skin effect in the analysis of the energy loss versus frequency is, however, available.

In this work, we investigate the dc and ac properties of Fe–(2 wt%)Si NO sheets and their frequency dependence up to 400 Hz as a function of compressive/tensile stress, applied in the range of $-30 \leq \sigma \leq +30$ MPa. The energy loss, measured at peak polarization values J_p ranging between 0.5 and 1.5 T, is shown to monotonically decrease while moving from compression to tension in the abovementioned range. Such a behavior is common to the quasi-static W_{hyst} and dynamic excess loss $W_{\text{exc}}(f)$ components, as expected to occur on general theoretical grounds [17]. This outcome can in fact be translated, according to the theory, in terms of statistical parameters of the magnetization process and their dependence on stress. However, with the increase of permeability induced by the tensile stress, skin effect phenomena do appear in the upper frequency range. They affect the relative proportions of the loss components versus frequency. Their calculation is made here, by determining the non-uniform cross-sectional

Manuscript received 22 March 2024; revised 28 June 2024; accepted 2 August 2024. Date of publication 7 August 2024; date of current version 26 September 2024. Corresponding author: C. Appino (e-mail: c.appino@inrim.it).

Color versions of one or more figures in this article are available at https://doi.org/10.1109/TMAG.2024.3439873.

Digital Object Identifier 10.1109/TMAG.2024.3439873

polarization profile versus frequency and the correspondingly evolving share of $W_{hyst}(f)$, $W_{exc}(f)$, and the classical loss $W_{class}(f)$.

II. Methods for Structural and Magnetic Characterization

This section is devoted to a description of the methods employed in the structural characterization and magnetic testing, with and without applied stress, of the high-purity NO Fe–Si alloys prepared in the Marcegaglia plant. Emphasis is placed, on the one hand, on crystalline structure and texture and, on the other hand, on the setup allowing for simultaneous tensile/compressive stress application and traceable magnetic measurements.

A. Structural Characterization

The NO Fe–Si sheets were prepared at Marcegaglia Ravenna plant starting from high-purity extra-low-carbon hot-rolled coils. The equivalent Si content in steel is about 2.0%. The final 0.50 mm-thick product was obtained by a sequence of pickling, cold rolling, and annealing processes. Epstein strips were eventually cut and stress-relieved by 2 h annealing at 680 °C in vacuum.

The structural investigation was made by optical and field-emission gun FEG-SEM microscopy. The SEM setup was endowed with energy-dispersive X-ray spectroscopy (EDS) and electron backscatter diffraction (EBSD) capabilities [18]. The optical micrographs show almost equiaxed grains, while the SEM micrographs, coupled with EDS analysis, put in evidence the presence of MnS inclusions. The results of EBSD analyses and post-processing are provided in Fig. 1.

High-angle grain boundaries (HAGB, $\theta > 15°$) are found to be prevalent with respect to low-angle grain boundaries (LAGB, $2° < \theta \leq 15°$). Combined with the absence of specific ordered structures in LAGB, this implies that the material has undergone almost complete recrystallization [19]. The inverse pole figure (IPF) reported in Fig. 2(a) shows that the [110] axes are the prevailing crystallographic axes pointing toward the rolling direction (RD), with a relatively high population of (557)[1$\bar{1}$0] and (335)[1$\bar{1}$0] orientations. At the same time, comparably few [001] axes tend to lie close to RD and the transverse direction (TD). Slight favorable anisotropy along RD is eventually demonstrated by magnetic measurements. Table I provides the basic physical parameters of the investigated laminations.

TABLE I
Physical Parameters of the Investigated Fe–Si Sheets

Thickness d (mm)	Average grain size $<s>$ (μm)	Resistivity ρ (Ωm)	Density δ (kg/m^3)	J_s (T)
0.498	102	$38.9 \cdot 10^{-8}$	7700	2.05

B. Magnetic Characterization

The magnetic measurements have been performed on 300 × 30 mm Epstein samples by means of a single-strip tester, endowed with a double-C flux-closing laminated yoke of cross-sectional area 30 × 30 mm [Fig. 3(a)]. The exciting field H_a is generated by a solenoid, and the flux derivative is detected by means of an air-flux compensated secondary coil located at sample mid-length. A defined magnetic path length is adopted by comparing the measurements at zero stress with the results obtained on a standard Epstein frame. The scattering between the results obtained by the single strip and Epstein frame magnetic circuits is within the systematic deviations found for the International Electrotechnical Committee (IEC) testing standards discussed in [20].

The compressive/tensile stress is applied to the strip under test by a built-on-purpose setup, endowed with a calibrated linear spring and a brass structure, holding the strip. Besides directly applying the tensile stress, this device can transform the pulling action of the spring into a compressive force on the strip. The strip is sandwiched between two brass sheets, one fixed and one mobile, which accomplish the tension-to-compression transition while averting buckling of the strip.

The dc magnetic properties are measured by the point-by-point (ballistic) method [21], each time repeating the test on the RD- and TD-cut strips and averaging the results. Fig. 4 summarizes the stress dependence of the so-obtained normal magnetization curves ($-30 \leq \sigma \leq +30$ MPa) up to the maximum applied field $H_a = 10$ kA/m. The normal and the anhysteretic curves measured on the Epstein frame (IEC 60404-2 Standard) in the unstressed state are additionally shown.

AC measurements are performed by means of a calibrated digital hysteresisgraph-wattmeter in the frequency range of 2–400 Hz under controlled sinusoidal secondary voltage at the peak polarization values $J_p = 0.5$, 1.0, 1.2, and 1.5 T. The measuring setup is based on a digital function generator (Agilent 33220A), a power amplifier (NF HSA 4052), and a 12-bit 200-MHz MSO44 Tektronix oscilloscope. It operates via an Agilent VEE software. A block diagram of the measuring setup is provided in Fig. 3(b).

The dependence of the quasi-static major hysteresis loops (RD strip, $J_p = 1.5$ T and $f = 1$ Hz) on the applied stress is shown in Fig. 5. The opposite trends of area and slope of the loops with σ changing from -30 to $+30$ MPa are apparent. These trends are quantified in Fig. 6, where the decrease of the area of the loop (i.e., the quasi-static energy loss W_{hyst}) is paralleled by the dramatic increase of the maximum value of the differential permeability $\mu_r^{(max)}$, taken on the ascending branch of the loop. We see here how the stress operates at the same time on the slope of the magnetization curve, via the cumulated magnetoelastic and demagnetizing energies, and the coercivity, that is, the frictional resistance to the motion of the dws. This will be discussed in detail in Section III. It is appropriate, in any case, to figure out how the measuring uncertainty associated with the present unconventional test methods is deteriorated with respect to the conventional

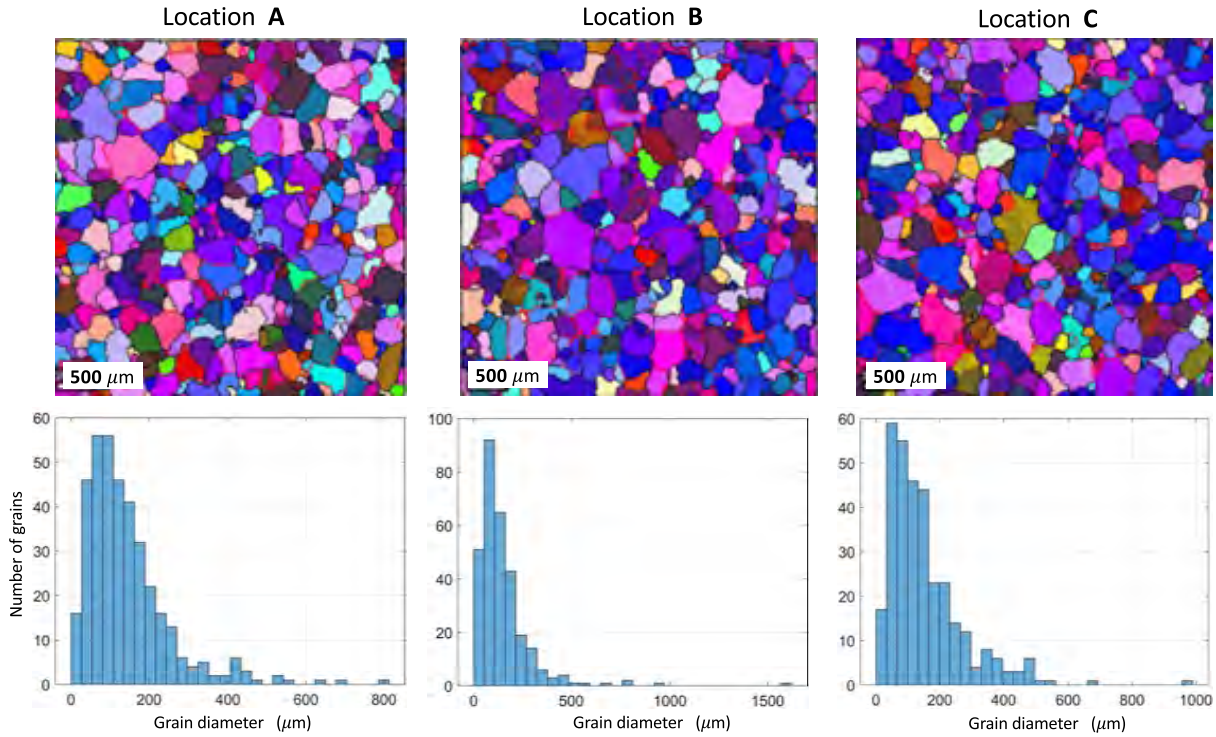

Fig. 1. Grain orientation distribution reconstructed by EBSD at three different locations of the NO Fe–Si sheet surface and corresponding distribution of the grain diameters. Prevalent large-angle grain boundaries are found.

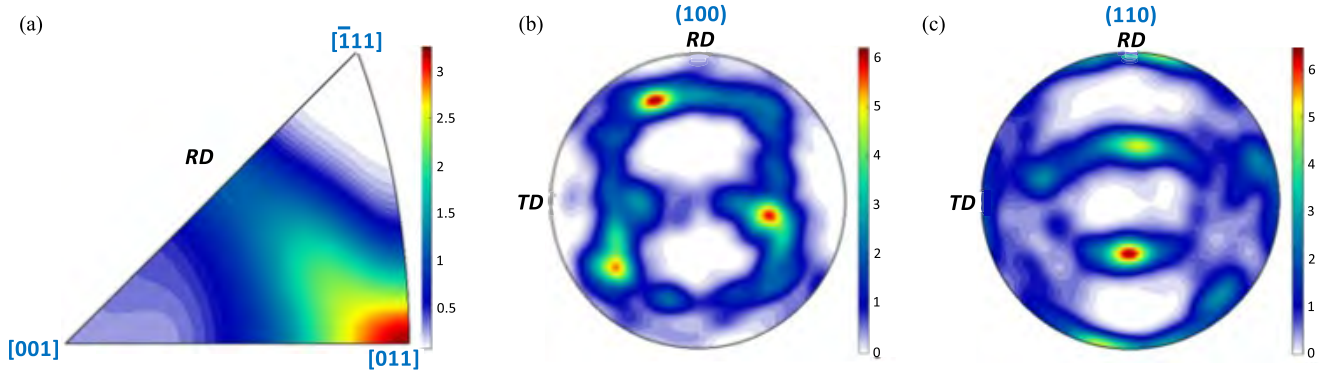

Fig. 2. Inverse pole figure. (a) Distribution of the crystallographic axes around the RD tends to be denser around the [011] axis, consistent with the (110) and (100) pole density figures shown in (b) and (c).

standard testing (e.g., Epstein frame). We identify, in particular, the main source of uncertainty of the loss figures in the systematic evolution with σ of the magnetic path length of the adopted single-strip setup. This is defined once and for all by comparison with the Epstein frame tester at $\sigma = 0$. Based on the historical record of the laboratory, previous intercomparisons, and the estimated evolution of the magnetic path length with the applied stress, the systematic extended uncertainty (Type B) is evaluated to range between $\pm 4\%$ and $\pm 7\%$. The random (Type A) contribution, reduced to low values (around 0.5%) by controlled repeated measurements, is deemed negligible.

III. Experimental Results and Discussion

The major and most investigated effect of residual and applied stresses on the magnetic properties of steel sheets is the modification of the quasi-static hysteresis, namely, the coercive field and the permeability. However, it has been shown that the statistics of the magnetization process, eventually regulating the dynamic evolution of the dw motion under increasing frequencies, connects quasi-static and dynamic losses, a phenomenon embodied in the so-called excess losses [17]. Remarkably, the theory permits one to separately analyze quasi-static and dynamic losses while bringing to light, at the same time, their intrinsic connection, as discussed in the following.

A. Quasi-Static Magnetic Properties

We can qualitatively understand the results reported in Section II-B by considering the mechanisms of the magnetization process in NO Fe–Si alloys in the presence of an applied field.

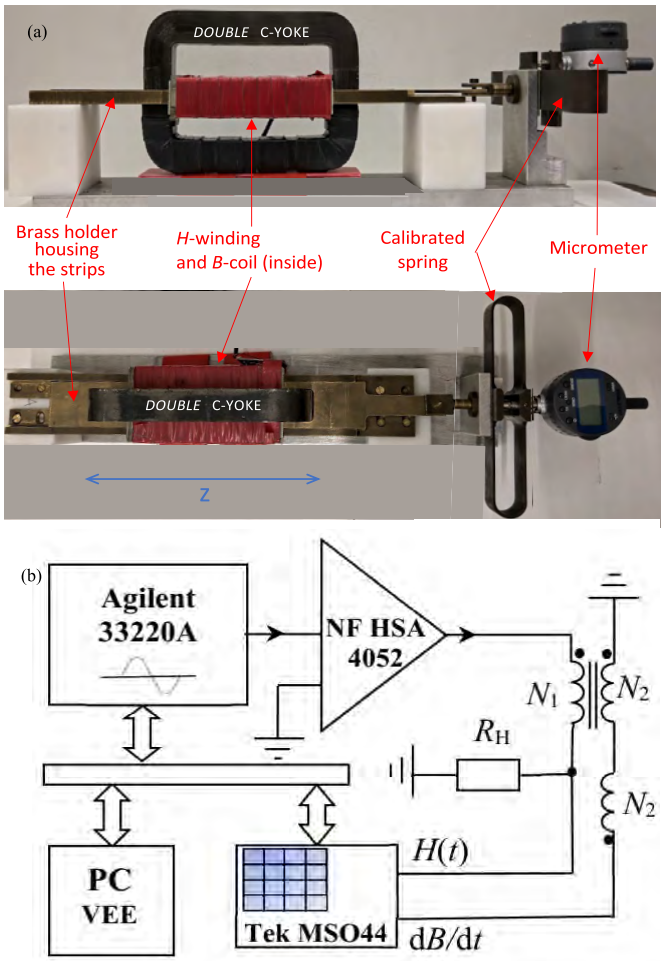

Fig. 3. Setup for the single-strip magnetic characterization of NO Fe–Si under tensile/compressive stress (applied along the z-direction, see Fig. 7). (a) Sample is housed in a brass holder, preventing strip buckling under compression. Flux closure is ensured by a double-C laminated yoke and the stress is applied using a calibrated linear spring. (b) Block diagram of the measuring setup. The air flux detected by the secondary winding (N_2) is compensated.

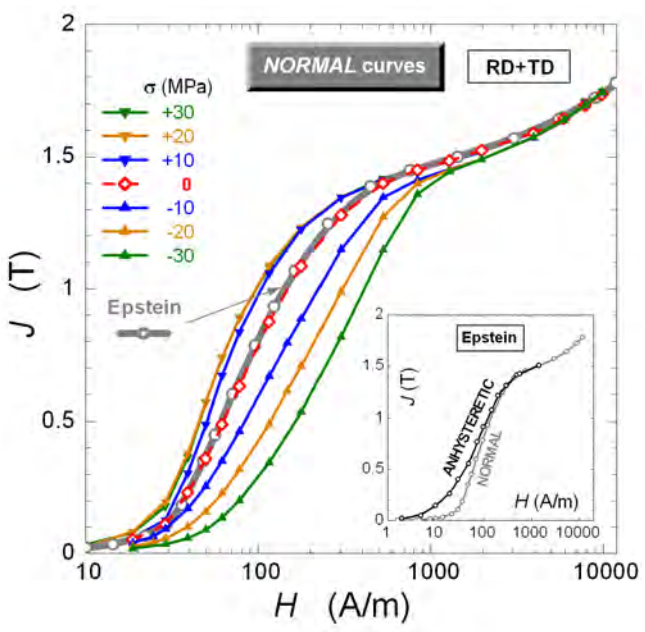

Fig. 4. DC magnetization curve versus applied compressive/tensile stress ($-30 \leq s \leq +30$ MPa). Each curve is the average of the curves measured on the RD and TD strips. The inset compares the normal and the anhysteretic curves, as obtained in the unstressed state (Epstein frame). The asymmetric response of the material to compression and tension points to a large difference of the correspondingly stored magnetoelastic energy.

Commercial NO Fe–Si sheets display, despite a respectably high value of the anisotropy constant [$K \sim 40$ kJ/m^3 in Fe–(2 wt%)Si], a relatively low coercivity, that is, a relatively easy motion of the dws, a property favored by the purity of the material and the positive cubic anisotropy. A certain inflection, therefore, sets in along the magnetization curve between the dw processes and the rotations, the latter requiring much higher fields. This is signaled by the peculiar transition region appearing on the log-lin normal curves shown in Fig. 4 upon overcoming the polarization value $J \sim 1.5$ T. In the ideal case of perfectly isotropic polycrystalline material, this transition would reflect the passage from dw motion to reversible moment rotations versus the applied field direction.

This should occur, in principle, inside a uniform distribution of occupied easy axis covering a solid angle of semi-aperture $\theta_0 = 55°$, centered on the field direction.

As is generally the case, a certain degree of anisotropy is observed in these NO sheets, as conveyed by the character of pole figures shown in Fig. 2. The angular distribution of the occupied easy axes is therefore not uniform, and moderate differences are always observed, for example, between the magnetization curves and the loops taken along RD and TD (inset of Fig. 5). Consequently, lower permeability and slightly higher losses are observed in the TD-cut strips. In addition, residual stresses and internal demagnetizing fields can lead, after demagnetization, to the further departure of the populated easy axes from the previously evoked ideal distribution.

The presence of a compressive ($\sigma < 0$) or tensile ($\sigma > 0$) applied stress perturbates this scenario, by modifying the distribution of the domains in the demagnetized state (while maintaining the sample demagnetized) and generating an asymmetric response (tension versus compression) upon the application of a magnetic field. A qualitative view of the distribution of the occupied ⟨100⟩ easy axes in the demagnetized state, after the application of either a tensile or compressive stress, is shown in Fig. 7. Because of the positive value of the saturation magnetostriction constant λ_s, the magnetization will tend to occupy the easy axis closer to or farther from the stress direction, according to the tensile or compressive character of the stress, to minimize the magnetoelastic energy E_σ. For a domain with magnetization directed at an angle θ with respect to the direction of σ, we have

$$E_\sigma(\theta) = \frac{3}{2}\lambda_s \sigma \sin^2\theta, \quad [\text{J/m}^3] \tag{1}$$

with σ expressed in pascal. It is apparent how the selection of the easy axes brought about by sign and amplitude of σ can lead to the evolution of the quasi-static hysteresis loops, their area, and the differential permeability observed in Figs. 5 and 6.

1) Tensile Stress: We can attribute the moderate magnetic softening ensuing from the tensile stress to the rearrangement

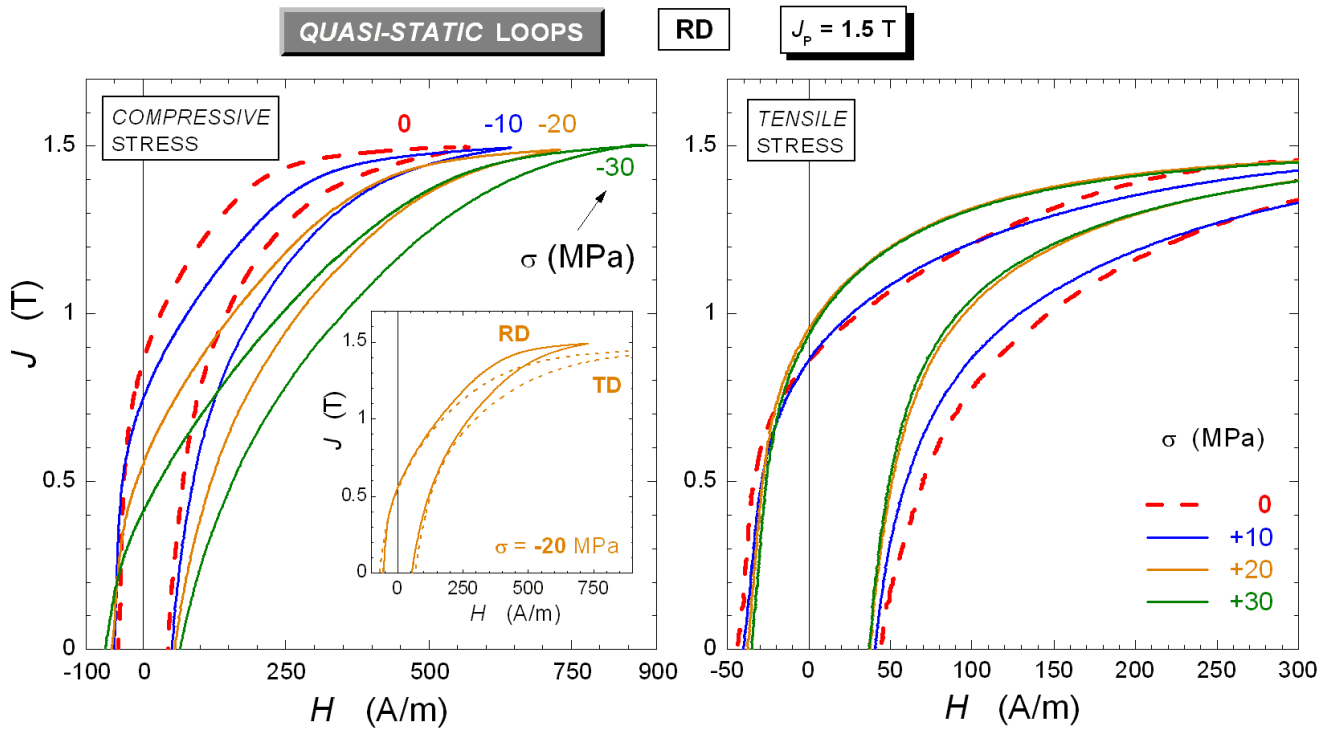

Fig. 5. Evolution of the major (J_p = 1.5 T) quasi-static hysteresis loop versus applied tensile/compressive stress in the RD strips. The inset shows an example of loops taken on RD and TD strips at the same J_p value.

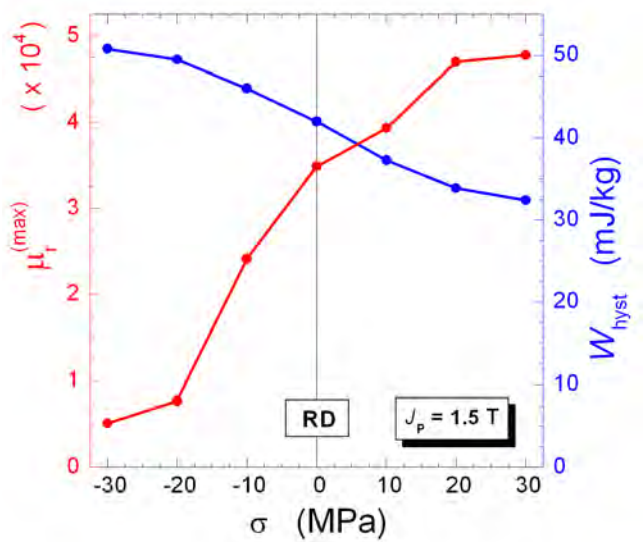

Fig. 6. Maximum value attained by the differential permeability $\mu_r^{(\max)} = (1/\mu_0)\, dJ/dH$ along the ascending branch of the quasi-static major loops (Fig. 5) decreases monotonically on passing from $\sigma = +30$ to -30 MPa. The opposite trend is displayed by the quasi-static energy loss W_{hyst}.

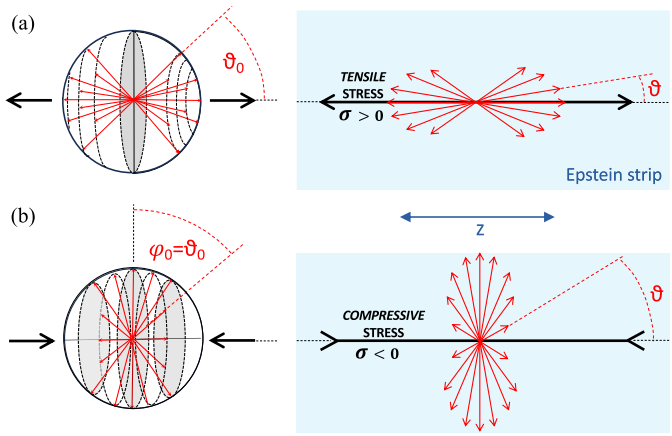

Fig. 7. Angular distribution of the active (i.e., occupied by the magnetization) easy axes in the polycrystalline NO Fe–Si specimen is sketched for the demagnetized state, once this is attained after the application of a tensile (a)/compressive (b) stress ($\theta_0 = \varphi_0 = 55°$). Rotational symmetry around the stress axis z is assumed. The field is applied collinear with σ.

of the domains along the pattern sketched in Fig. 7(a), starting from the somewhat broader range of occupied orientations usually expected to occur in the zero-σ state. With the easy axes closer to the applied field direction, (1) leads, in combination with reduced internal magnetostatic fields, to a decrease of the energy required to achieve a defined J_p level. This trend tends to saturate already around $\sigma = +30$ MPa and it is expected to eventually reverse upon further increase of σ, up to the yield strength [7], [8]. The ensuing magnetic hardening is primarily due to the lack of degrees of freedom (i.e., flux-closing domains) at high stresses and correspondingly hindered propagation of the magnetization reversals. Additional non-negligible contribution to the magnetocrystalline anisotropy from the stress-induced anisotropy will eventually appear before yield.

2) Compressive Stress: There is an obvious geometrical effect leading to higher coercivity and hysteresis loss under compressive stress in polycrystalline materials because, as far as the 180° dws remain anchored to or fall back along the easy axes far-removed from the direction of the applied field (i.e., of the stress), the pressure $p = 2HJ_s \cos\theta$ on the 180° dws

is relatively ineffective. Switching between easy axes, driven by 90° dw processes, is needed to establish, in each grain, the domain structure lying along the axes closer to the field direction. The threshold for this process is responsible, besides the increase of the hysteresis loss W_{hyst}, for loop bulging, a known consequence of compressive stress and plastic deformation [5], [6], [15], [16], [22], [23]. We therefore see in Fig. 8(a) how the major quasi-static hysteresis loop measured for $\sigma = -30$ MPa is inflated in the region surrounding the coercive field, where the 90° dw transitions take place. It is further observed in Fig. 8(b) that for compressive σ larger than -10 MPa, the loops exhibit a common crossover point in the second and fourth quadrants, as reported in [6], [15], [16], and [22].

We might phenomenologically look at the remarkable effect of the compressive stress on the shape and area of the quasi-static hysteresis loop in NO Fe–Si sheets by considering the overall energy balance and separating the lost fraction W_{hyst} from the reactive contribution, reversibly exchanged between the sample and the exciting system. We consider in Fig. 9(a) the upper portion of the quasi-static major loops for $\sigma = 0$ and $\sigma = -30$ MPa and the related median curves. These are akin to, but not coincident with, the anhysteretic curves and are assumed to describe the evolution of the reactively exchanged energy during cycling, the frictional field being lumped, for any J value, in the half-width of the loop. Loop bending engendered by compression is therefore assumed to chiefly descend from the rise of the magnetoelastic and demagnetizing energies (i.e., the corresponding internal fields). We can estimate the former, for the relatively high $\sigma = -30$ MPa stress value, by considering the active easy axes configuration sketched in Fig. 7(b). We calculate the related magnetoelastic energy E_σ before and after application of a field, collinear along the z-axis with the stress, bringing the magnetization up to $J_p = 1.5$ T. The xy plane is, from the viewpoint of magnetoelastic energy, an easy plane. It is fair to stress the somewhat ideal character of the scheme adopted in Fig. 7, for the distribution of the populated easy axes that is likely more complex in practice, as induced by the observed textural properties of the material. We make use of (1) to calculate E_σ, according to the distribution sketched in Fig. 7(b) (semi-aperture $\varphi_0 = 55°$) corresponding to the demagnetized state under compression. By denoting as φ the angle made by the generic occupied easy axis with the xy plane and assuming uniform density, we obtain the distribution $p(\varphi) = \cos\varphi/\sin\varphi_0$ by integration

$$E_\sigma^{(-30\,\text{MPa})}(J=0) = \int_0^{\varphi_0} E_\sigma(\varphi)p(\varphi)\text{d}\varphi = \frac{1}{2}\lambda_s\sigma\sin^2\varphi_0 \cong 0.33\lambda_s\sigma. \quad (2)$$

We similarly calculate E_σ at the tip point ($J_p = 1.5$ T), by assuming that the applied field has brought the distribution very close to the one depicted in Fig. 7(a) (corresponding also to the one pertaining to the demagnetized state with $\sigma = 0$) with $\theta_0 = 55°$. It is now $p(\theta) = \sin\theta/(1-\cos\theta_0)$ and the integration provides

$$E_\sigma^{(-30\,\text{MPa})}(J=1.5\text{ T}) = \int_0^{\theta_0} E_\sigma(\theta)p(\theta)d\theta = \frac{1}{2}\lambda_s\sigma(\cos^2\theta_0 + \cos\theta_0 + 1) \cong 0.95\lambda_s\sigma. \quad (3)$$

We conclude that on passing from the demagnetized state to $J_p = 1.5$ T, the magnetoelastic energy increases by the quantity $\Delta E_\sigma^{(-30\,\text{MPa})} = E_\sigma^{(-30\,\text{MPa})}(J = 1.5\text{ T}) - E_\sigma^{(-30\,\text{MPa})}(J = 0) \cong 0.62\lambda_s\sigma$. With $\lambda_s = 8 \times 10^{-6}$, we obtain $\Delta E_\sigma^{(-30\,\text{MPa})} \cong 148$ J/m^3, a figure affected by the uncertainty attached to the assumed λ_s value. We compare this estimate with the integrals $E_r = \int_0^{J_p} H dJ$ taken on the median curves of the $J_p = 1.5$ T loops for both $\sigma = 0$ and $\sigma = -30$ MPa. These provide a measure of the reactive energy exchanged with the supply system. It is $E_r^{(\sigma=0)}(J = 1.5\text{ T}) \cong 135$ J/m^3 and $E_r^{(-30\,\text{MPa})}(J = 1.5\text{ T}) \cong 430$ J/m^3. The latter is shared between the magnetostatic and magnetoelastic contributions. By assuming that the reactive energy in the unstressed state $E_r^{(\sigma=0)}(J = 1.5\text{ T})$ is of magnetostatic origin, we find the global demagnetizing energy cumulated at $J_p = 1.5$ T for $\sigma = -30$ MPa and $E_{\text{dem}}^{(-30\,\text{MPa})}(J = 1.5\text{ T}) \cong 282$ J/m^3.

We might treat the problem, for any J value, in terms of balance between applied field H_a and internal fields

$$H_a = H_f + H_{\text{dem}} + H_\sigma \quad (4)$$

where H_a is countered, besides the demagnetizing H_{dem} and stress $H_\sigma = dE_\sigma/dJ$ fields, by the frictional field H_f. This, like the other fields, is treated like a macroscopic quantity, embodying the energy $dW_{\text{hyst}} = H_f dJ$ lost upon a variation dJ of the polarization. We have

$$W_{\text{hyst}} = \oint H_a dJ = \oint H_f dJ. \quad (5)$$

If the major hysteresis loops in Figs. 8 and 9(a) are deprived of the field contribution, sum of H_σ and H_{dem}, associated with the median curves [Fig. 9(b)], we remain with the hypothetical $J(H_f)$ loops, lumping all the dissipative responses of the material [Fig. 9(c)]. By limiting ourselves to the return curves, we obtain by subtraction the $J(H_f)$ branches, ranging from $\sigma = 0$ to $\sigma = -30$ MPa, represented in the second quadrant in Fig. 9(c). The peculiar bulging of H_f shows up, inflating and moving downward under increasing compressive stress σ. This signals that the populated easy axes distribution concurrently moves between the two ideal configurations shown in Fig. 7. It is noted in Fig. 9(c) the separation of the hysteresis curves about the coercive field H_c in their irreversible (solid lines) and reversible (median curves—dashed lines) components. The latter tend to fall, for compression larger than $\sigma = -10$ MPa, through a common crossover point. This denotes the existence of an inverse relationship between the slope of the pertaining median curves and the extra-contribution ΔH_c due to the compressive stress. The higher the increase of coercivity by compression, the lower the slope of the median curve.

B. AC Properties and Loss Separation

As previously remarked, the hysteresis and the dynamic losses are affected in a connected fashion by tensile\compressive stresses. A way to recognize this correlation consists in retrieving the excess loss component,

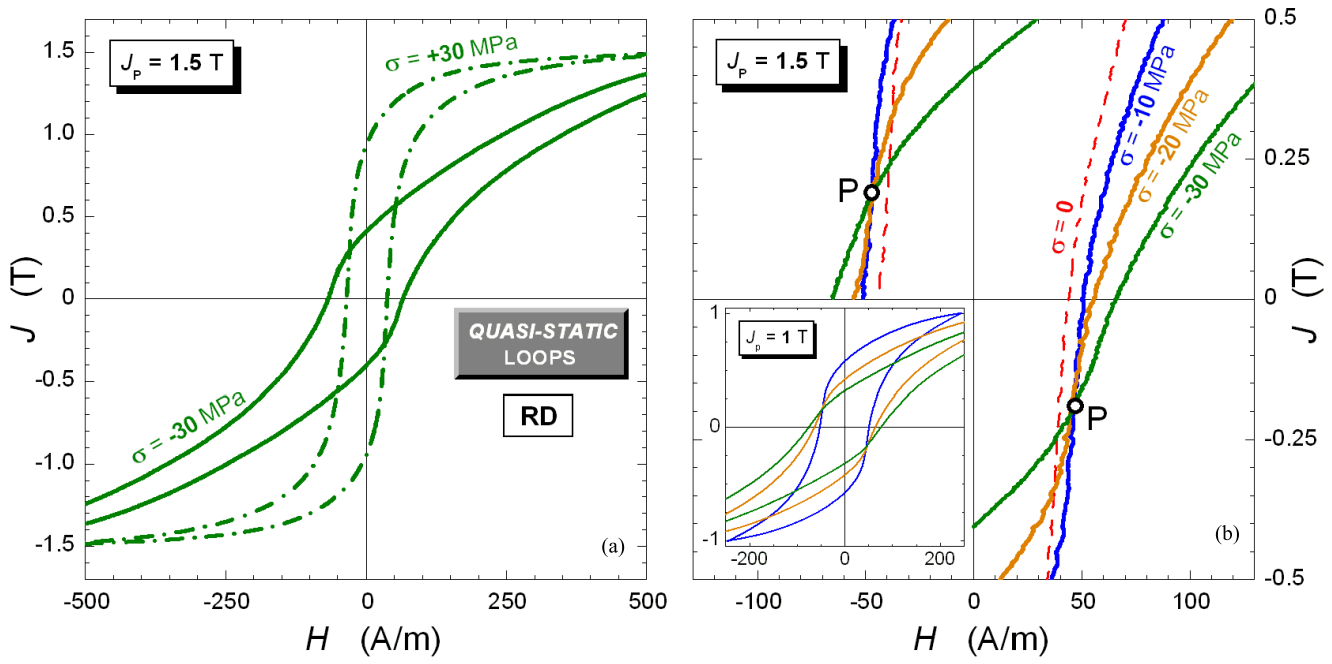

Fig. 8. (a) Close look at the quasi-static loops shown in Fig. 4 provides evidence that compression engenders a considerably inflated shape around the coercive field. It descends from the extra-pressure required for the switching of the magnetization between different easy axes, a process taking place by 90° dw transitions. Magnetoelastic energy is stored in this process, resulting in loop bending. (b) Magnified detail of crossover for $J_p = 1.5$ T and the inset ($J_p = 1.0$ T) show that under sufficiently high compressive stress and appropriate J_p value, all the quasi-static loops tend to crossover at a common (H, J) value (P) in the second and fourth quadrant.

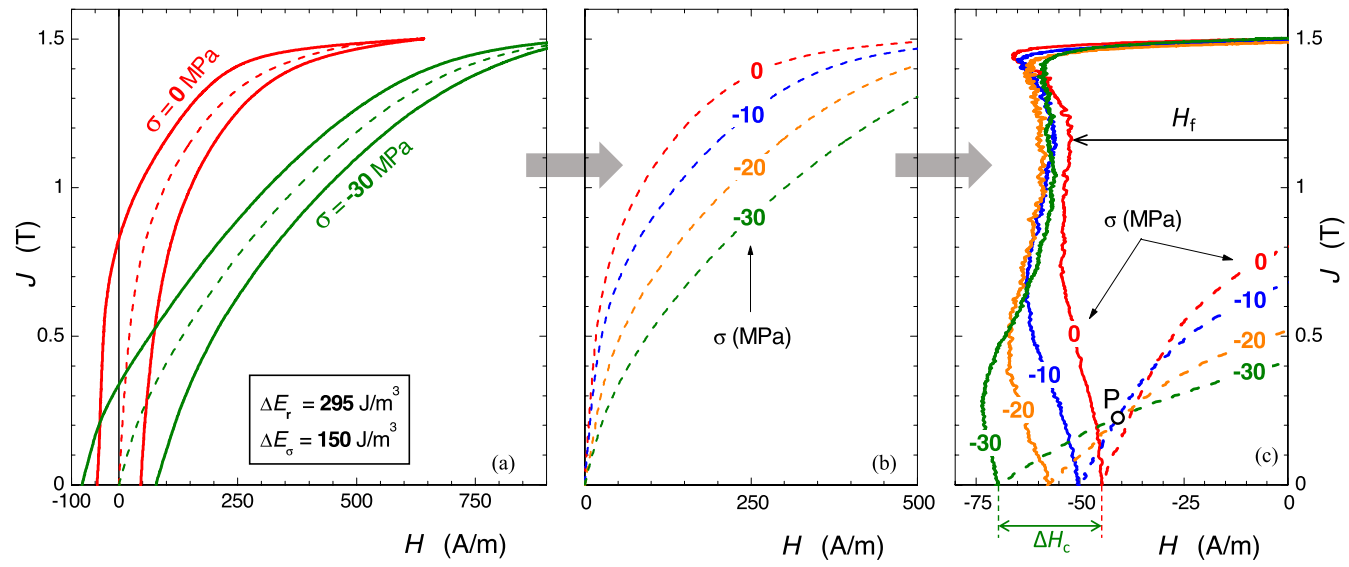

Fig. 9. RD sample. (a) Median curves $J_m(H)$ of the quasi-static major hysteresis loops (dashed lines) are representative of the reactive (reversible) energy $E_r(J_m) = \int H dJ_m$ involved in the cycling process. We assume E_r as the sum of two contributions: a term E_{dem}, associated with the internal demagnetizing effects, and a quantity E_σ, introduced by the magnetoelastic interaction. We estimate in (a) the variation of E_r and E_σ, cumulated up to $J_p = 1.5$ T, on passing from $\sigma = 0$ to -30 MPa, by resorting to the easy axes scheme shown in Fig. 7. By subtracting the median curves shown in (b) (first quadrant) to the hysteresis loops at different compressive stress values, the dissipative contribution (H_f, J), with H_f the frictional field, is singled out in the second quadrant and the bulge concurrent with the switching of the magnetization between easy axes by 90° dw processes is revealed in (c). The dashed lines in the second quadrant (c) are partial replicas of the median lines shown in the first quadrant (b). Their crossover suggests the existence of an inverse relationship between the stress-induced coercivity and the slope of the median curves.

the quantity providing a measure of the discrete nature of the magnetization process, and its evolution with the magnetizing frequency. We will discuss this in the following, by additionally treating, with certain simplifications, the rise of the skin effect, which cannot be neglected when the product of frequency and permeability is sufficiently high.

The energy loss $W(J_p, f)$ measured in the NO Fe–Si sheets from dc to 400 Hz (RD + TD) at different peak polarization values ($J_p = 0.5$, 1.0, 1.2, and 1.5 T) increases

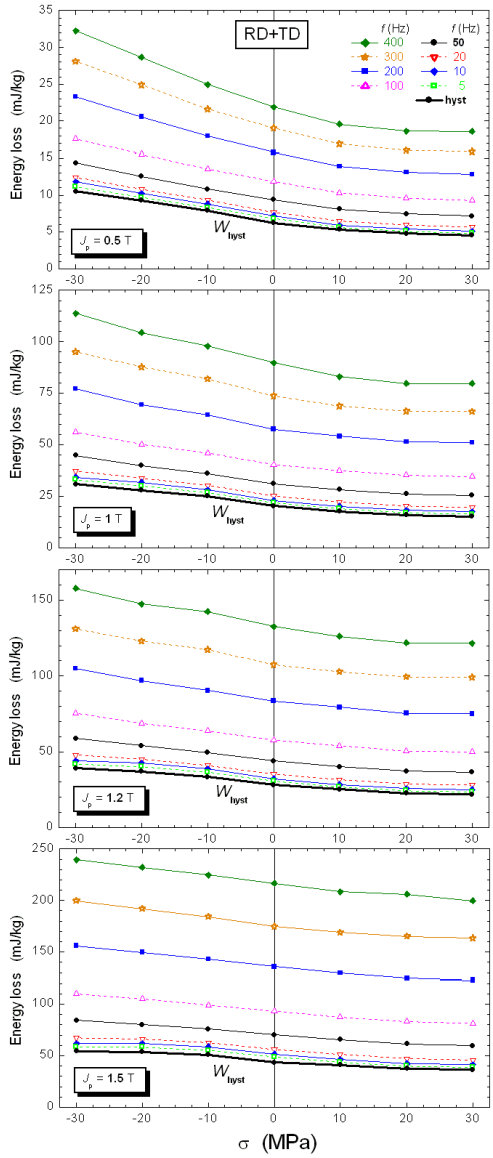

Fig. 10. Measured energy loss in the NO Fe–(2 wt%)Si sheets increases monotonically on passing from tensile to compressive stress at all frequencies and peak polarization values.

monotonically on passing from tensile to compressive stress across the whole investigated (J_p, f) matrix. This is illustrated by the comprehensive data reported in Fig. 10. As already observed in Fig. 6 for W_{hyst}, the rate of variation of $W(\sigma)$ tends to saturate toward $\sigma = \pm 30$ MPa, at least up to 50 Hz, while the major detrimental effect of compression is found at $J_p = 0.5$ T. This is an expected result, because the permeability in the unstressed state peaks at this J_p value.

The frequency dependence of the energy loss in steel sheets is conveniently approached through modeling of the magnetization process by the statistical theory of losses (STL) [17], [24]. This approach provides solid ground to the concept of loss separation, where the energy loss is derived as the sum of the previously discussed quasi-static component W_{hyst} and the dynamic classical $W_{\text{class}}(f)$ and excess $W_{\text{exc}}(f)$ loss components. The physical interpretation of the loss separation is based on a critical analysis of the mechanisms of the magnetization process and their evolution with the magnetizing frequency. It is assumed according to the experimental evidence provided by the Barkhausen effect that the magnetization process is driven by randomly distributed statistically independent regions named magnetic objects (MOs), each accounting for the role played by a dw or group of strongly interacting dws. The sequence by which the MOs are activated depends on the balance between the uniformly applied magnetic field H_a and the local fields (pinning, magnetostatic, magnetoelastic, and eddy current fields). To manage the complex statistics of the problem, it is assumed that the local pinning fields $H_c^{(\text{loc})}$ are homogeneously distributed throughout the cross section of the sheet, up to a maximum value H_0 (probability density function $g(H_c^{(\text{loc})}) = 1/H_0$). At any frequency, n of the total N_0 of MOs, separated one to another, on average, by a field increment $V_0 = H_0/N_0$, is assumed to be simultaneously reversing the magnetization. n is bound to increase with f because the eddy current counterfields call for increased H_a, if the defined J_p value and dJ/dt law (e.g., sinus) are to be preserved. Additional MOs are therefore recruited by the larger H_a. It is shown by Bertotti [17], [24] that in steel sheets, the linear relationship

$$n = n_0 + H_{\text{exc}}/V_0 \tag{6}$$

holds, where $H_{\text{exc}} = W_{\text{exc}}/4J_p$ and n reduces to n_0 for $f \to 0$.

Simplified in this way, the arduous problem of dynamic losses is amenable to simple analytical assessment, with the components given, for sinusoidal $J(t)$ in a sheet of thickness d, by the expressions

$$W_{\text{class}}(J_p, f) = (\pi^2/6\rho)d^2 J_p^2 f \quad [\text{J/m}^3] \tag{7}$$

$$W_{\text{exc}}(J_p, f) = 2n_0 V_0 J_p\left(\sqrt{1+\frac{16}{\rho n_0^2 V_0}GSJ_p f}-1\right), \quad [\text{J/m}^3] \tag{8}$$

where ρ is the resistivity and $G = 0.1356$. The less-than-linear increase of $W(f)$ is predicted by (8). Since the memory of the quasi-static situation is progressively lost as the frequency increases, (8) generally simplifies, beyond a few Hz, into the well-known square root dependence of W_{exc} on frequency

$$W_{\text{exc}}(J_p, f) = 8.76\sqrt{GSV_0/\rho}\,J_p^{3/2}\sqrt{f} \quad [\text{J/m}^3]. \tag{9}$$

We see the interpretative approach offered by STL at work in the examples given in Fig. 11, where $W(f)$, measured up to 400 Hz at $J_p = 1.5$ T under the symmetric stress conditions $\sigma = \pm 30$ MPa, is decomposed according to (7) and (9). The correspondingly obtained $n(H_{\text{exc}})$ (inset) is shown to obey the linear law (6) and the measured $W(f)$ (symbols) is eventually predicted (solid line) as $W(f) = W_{\text{hyst}} + W_{\text{class}}(f) + W_{\text{exc}}(f)$. To note that W_{hyst} and $W_{\text{exc}}(f)$ follow the same trend with σ, bringing forth the known relationship existing between quasi-static and dynamic losses.

1) Skin Effect: The pre-requisite of uniform flux density (i.e., skin depth larger than $d/2$) for calculating $W_{\text{class}}(f)$ with (7) may not be fulfilled for certain combinations of conductivity, permeability, and sheet thickness, even at power

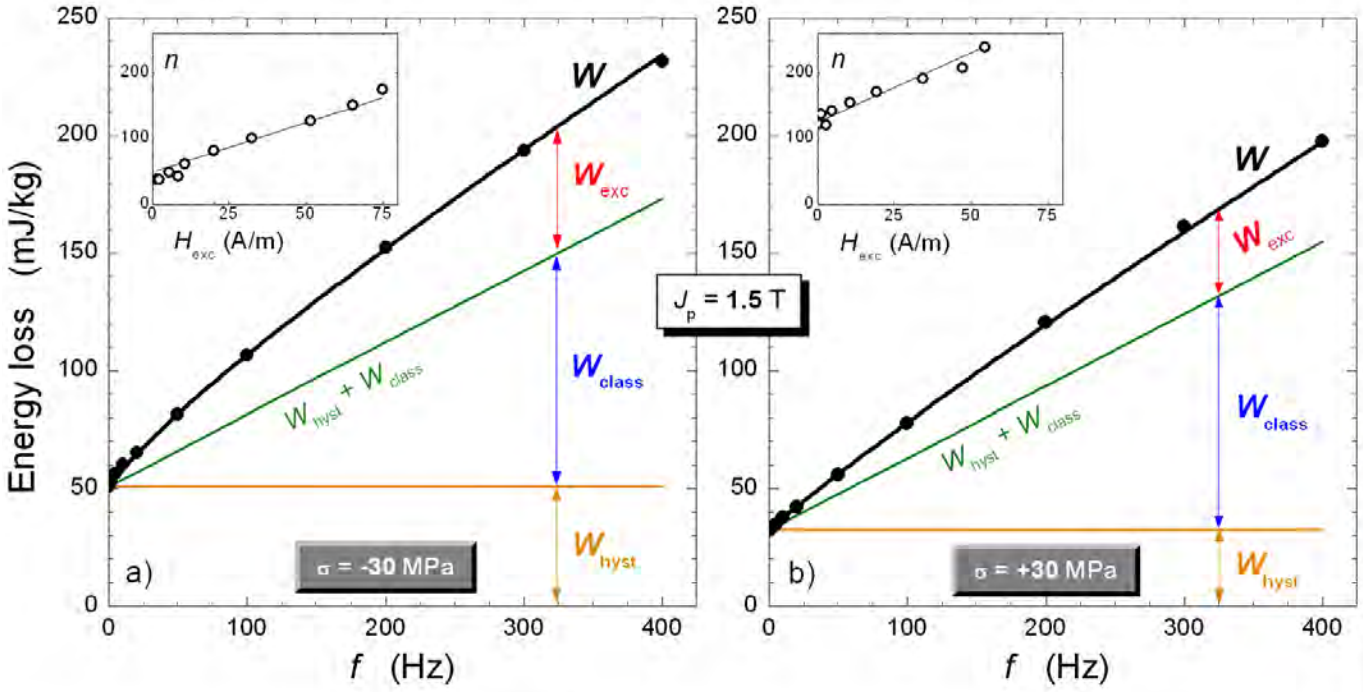

Fig. 11. Energy loss $W(f)$ measured at $J_p = 1.5$ T for $\sigma = \pm 30$ MPa (symbols) on an RD specimen is decomposed in the W_{hyst}, W_{class}, and W_{exc} components. W_{hyst} is obtained by extrapolating $W(f)$ to $f = 0$ and $W_{\text{class}}(f)$ is calculated with (7). The remainder is the excess loss W_{exc}, obtained with (9), following an $f^{1/2}$ dependence. The sum of these three components (the black solid curves) fits the experiments to an extent demonstrating that the skin depth is large enough to assume a uniform induction level across the sheet thickness. The insets in (a) and (b) show that the calculated number of MOs $n(H_{\text{exc}})$ (symbols) follows with good approximation of the linear law (6).

frequencies. This is what occurs in the present 0.50 mm-thick sheets for tensile stress $\sigma \geq 10$ MPa, $f \geq 200$ Hz, and $J_p = 0.5$–1.0 T, where the use of (6) for $W_{\text{class}}(f)$ leads to incompatible behavior of $W_{\text{exc}}(f)$. This does not put the concept of loss separation in jeopardy, but it calls for the calculation of the actual profile $J(x)$ across the sheet thickness and the ensuing re-formulation of the dynamic loss. The problem was solved in the past, in the framework of loss decomposition, by numerical solution of Maxwell's diffusion equation in a material endowed with rate-dependent hysteretic magnetic constitutive equation, as given by the dynamic Preisach model [25]. However, it was shown that one can arrive at an acceptable assessment of the loss in the presence of skin effect, at the cost of a somewhat restricted (J_p, f) range (e.g., up to a few kilohertz, far from saturation), by identifying the magnetic constitutive equation with the elliptical loop having same J_p, and H_p values and same area as the actual quasi-static loop [26], [27]. This amounts to say that the loop is defined, besides H_p and J_p, in terms of real μ' and imaginary μ'' permeabilities. With the defined quasi-static μ' and μ'' values, the field diffusion equation for sinusoidal $J(t)$ is

$$\partial^2 \bar{H}(x)/\partial x^2 = \frac{1}{\rho}\partial \bar{J}(x)/\partial t = j\frac{\omega}{\rho}\bar{\mu}\bar{H}(x) \tag{10}$$

where $\bar{H}$, $\bar{J}$, and $\bar{\mu}$ are complex quantities and no distinction is made between magnetic polarization and induction. Following the detailed discussion given in [27], under the boundary conditions:

$$(\partial H/\partial x)_{x=0} = 0, \quad (\partial H/\partial x)_{x=\pm\frac{d}{2}} = \frac{d}{2\rho} j\omega\sigma J_p \tag{11}$$

where $J_p = \frac{2}{d}\int_0^{d/2} J_p(x)dx$ is the thickness-averaged (i.e., measured) peak polarization value, we calculate the profile $J_p(x, f)$, the classical loss $W_{\text{class}}(f)$, and the frequency-dependent W_{hyst}. These quantities are shown in Fig. 12(a) for $J_p = 0.5$ T and $\sigma = +30$ MPa, a measuring condition affected by incomplete skin depth. The theory [27] modifies (7) into

$$W_{\text{class}}(J_p, f) = \frac{\pi}{2}\frac{J_p^2}{\mu'} \cdot \frac{(\lambda' + \lambda'')\sinh(\lambda' - \lambda'') - (\lambda' - \lambda'')\sin(\lambda' + \lambda'')}{\cosh(\lambda' - \lambda'') - \cos(\lambda' + \lambda'')} \quad [\text{J/m}^3] \tag{12}$$

where

$$\lambda' = (d/2)\sqrt{\frac{\omega}{\rho}|\mu|} \cdot \sqrt{1 + \mu'/|\mu|}$$
$$\lambda'' = (d/2)\sqrt{\frac{\omega}{\rho}|\mu|} \cdot \sqrt{1 - \mu'/|\mu|}. \tag{13}$$

The so-calculated $W_{\text{class}}(f)$ displays, in the example shown in Fig. 12, a less-than-linear dependence on frequency beyond $f \sim 200$ Hz. This behavior is caused by the decreased intensity of the peripheral eddy currents under non-uniform $J_p(x)$ profile. This is responsible, at the same time, for a certain increase of the hysteresis loss W_{hyst} with f [see Fig. 12(b)]. $W_{\text{hyst}}(f)$ is generated by very localized dw processes and, exhibiting a more than linear dependence on J_p, is expected to grow with increasingly non-uniform $J_p(x)$ profile [e.g., on passing from 50 to 400 Hz in the example of Fig. 12(a)]. The experiments show that $W_{\text{hyst}}(J_p)$ follows under quasi-static excitation a power law dependence $W_{\text{hyst}}(J_p) = kJ_p^{\alpha}$ on J_p. For the case shown in Fig. 12, it is $\alpha = 1.86$ and $k = 14.87$

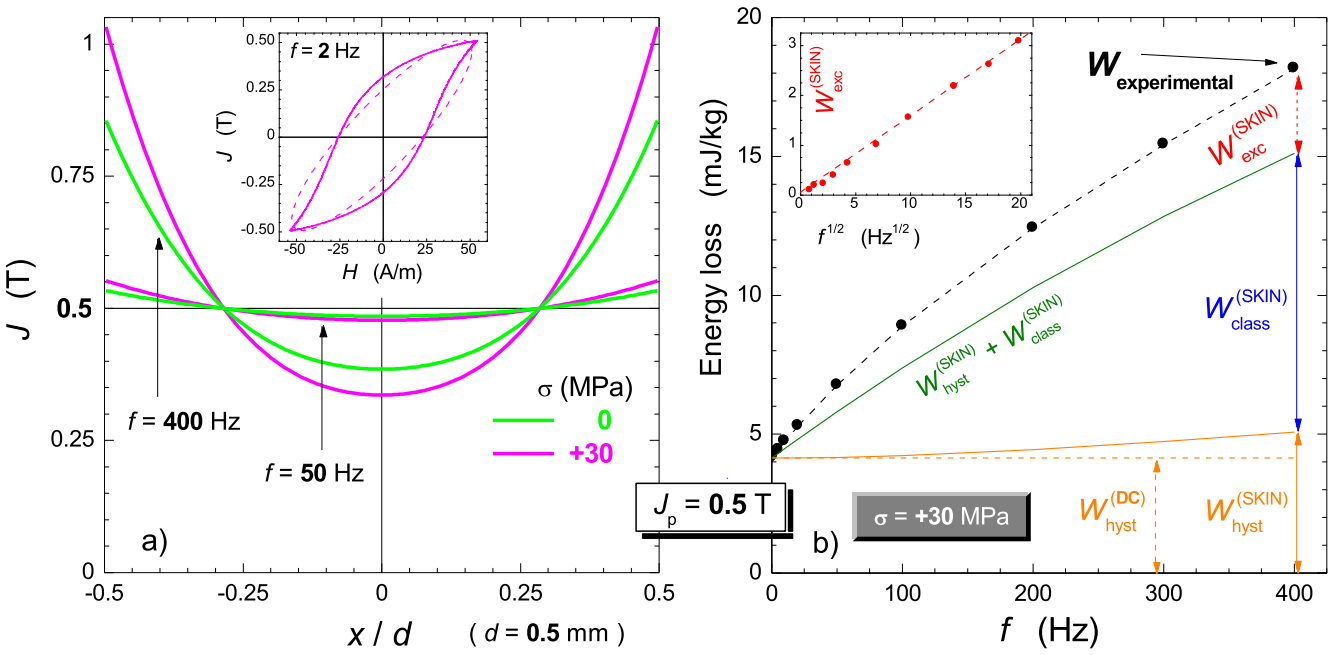

Fig. 12. Quasi-static hysteresis loop measured at $J_p = 0.5$ T on an RD specimen is assimilated to an elliptical loop of identical area, which can be described in terms of real μ' and imaginary μ'' permeabilities. This permits one to analytically solve Maxwell's diffusion equation and obtain both the $J_p(x, f)$ profile versus (a) depth x and (b) $W_{\text{class}}(f)$ in the presence of the skin effect. Because of non-uniform $J_p(x)$ profiles, W_{hyst} becomes, beyond a few hundreds of hertz, frequency-dependent, and $W_{\text{class}}(f)$ increases less than linearly with f.

(for W_{hyst} expressed in mJ/kg). Consequently, we find at any frequency

$$W_{\text{hyst}}(J_p, f) = \frac{1}{d}\int_{-d/2}^{d/2} k J_p^{\alpha}(x)dx \tag{14}$$

by integrating on the profile. We therefore see how the less-than-linear increase of $W_{\text{class}}(f)$ is paired by an increase of W_{hyst} with increasing f, with $W_{\text{exc}}(f)$ still approximately following the $f^{1/2}$ law [inset in Fig. 12(b)]. However, note that $W_{\text{class}}(f)$ will eventually reverse its trend with f for a suitable combination of high frequencies and high induction values, not attained in the present experiments [28].

C. Excess Loss and Statistical Parameters Versus Stress

The concept of loss separation and its assessment by the STL bring to light the physical mechanisms lying behind the generation of the excess losses, lumping them in the statistical parameters n and V_0 of the MOs and their mutual relationship (6). Such statistics is simplified, as previously mentioned, by assuming a uniform distribution of the strength of the local pinning fields [17]. The notion of locality implies that macroscopic demagnetizing effects do not interfere with the statistics and the loss. The resulting (somewhat idealized) parallelogram-shaped quasi-static hysteresis loop has the coercive field $H_{\text{hyst}} = W_{\text{hyst}}/4J_p$ and peak field value $H_{\max} = 2H_{\text{hyst}}$. Looking back at a similarly idealized major loop and its representation in the second quadrant in Fig. 9(c), we might approximately identify H_{hyst} with the frictional field H_f.

Whatever the degree of simplification, it is apparent that, by revealing the role of the parameters associated with the distribution of the local coercivities in the predictive formulations of the excess loss, we recognize the connection between W_{hyst} and W_{exc}. These two components are therefore expected to follow related trends under the effect of applied and residual stresses, which is exactly what we observe in the example of Fig. 13, showing the similar monotonic dependence of W_{hyst} and $W_{\text{exc}}(f = 50\text{ Hz})$ on σ at four different J_p values. Fig. 11 provides a clear example of the concurrent increase of W_{hyst} and $W_{\text{exc}}(f)$ upon changing σ from $+30$ to -30 MPa.

Use of (6)–(9) permits one to recognize the role of the parameters V_0 and $n(f)$ and their connection with the material microstructure. Equation (9) exclusively binds the dependence of $W_{\text{exc}}(f)$ on σ to the corresponding variation of V_0. This parameter marks the granularity (inhomogeneity) of the distribution of the local coercivities of the MOs, and within the scheme of their uniform distribution, it is quite appropriately found to follow the route taken by the upper limit H_0, that is of W_{hyst} (Fig. 13). The parameter V_0 is the *trait d'union* between W_{hyst} and W_{exc}, justifying their common response to stress application. Thus, a widened distribution subtends to a more granular structure and the increase of H_0 and V_0 under increasing compression. This is consistently accompanied, at any frequency, by a decrease of $n(f)$ (Fig. 13), that is, by the growing mean size λ_{MO} of the concurrently reversing MOs. λ_{MO} can be estimated versus the sign and amplitude of σ according to the derivation made in [29]

$$\lambda_{\text{MO}} = W_{\text{exc}} \Big/ \left(8.76 J_p \sqrt{\frac{2}{\rho}\langle J_s\rangle H_{\text{hyst}} f}\right) \tag{15}$$

where $\langle J_s\rangle = 0.83 J_s$ is the upper polarization limit at the (ideal) boundary separating dw processes and rotations. The

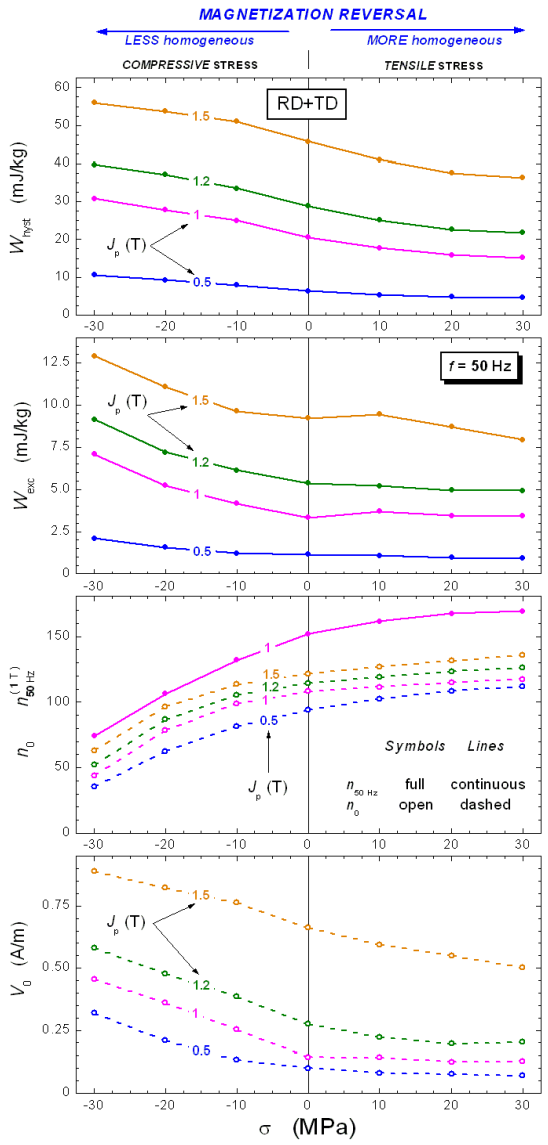

Fig. 13. Quasi-static and the excess loss components display similar trends under changing applied stress. These behaviors are predicted by the STL, via the statistical analysis of the magnetization process. The theory lumps the correlation between $W_{\rm hyst}$ and $W_{\rm exc}(f)$ in the distribution of the local pinning fields for the MOs and the related parameters V_0 and $n(f)$. The passage from tensile to compressive stress brings about a widened distribution of the local coercivities (increasing V_0) and an increased discretization of the active MOs [i.e., decreasing $n(f)$].

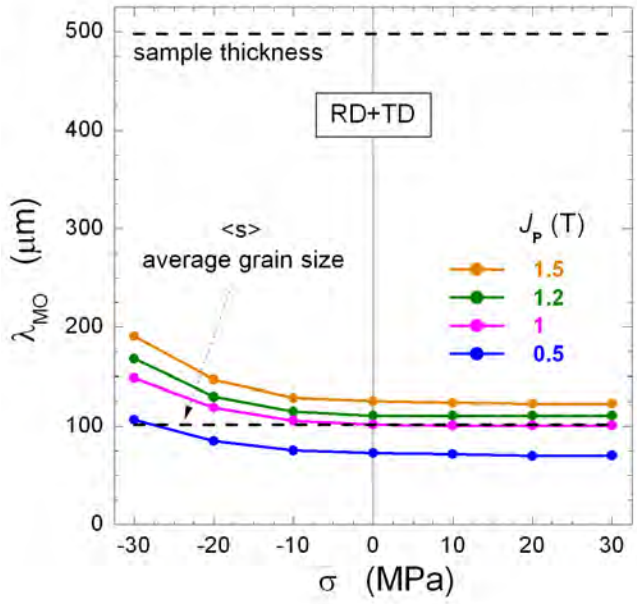

Fig. 14. Average size $\lambda_{\rm MO}$ of the reversing MOs increases on passing from tensile to compressive stress. $\lambda_{\rm MO}$ denotes the correlation range of the moving dws. It oscillates around the average grain size and it depends on J_p. The larger value engendered by $\sigma < 0$ reflects the rise of the threshold field for reversal when this requires the supplementary role of the 90° dws for magnetization switching between the easy axes.

so-calculated $\lambda_{\rm MO}$ value, shown versus σ in Fig. 14, is of the order of grain size. It increases under increasing compression ($\sigma < 0$), pointing to a dw correlation range growing with the growth of the barriers to be overcome in setting forth the combination of 90° and 180° dw motion.

IV. Conclusion

The lattice strain caused by an applied stress makes the orientation distribution of the magnetic domains among the easy axes sensitive to the tensile/compressive character of the stress, depending on sign and value of the magnetostriction constant. NO Fe–Si sheets, endowed with positive magnetostriction, have their domains in the demagnetized state prevalently distributed along the directions close either to the stress direction, if tensile, or to the plane orthogonal to it, if compressive. This favors the magnetization process under tensile stress while hindering it under compression, resulting into monotonical increase of hysteresis (quasi-static) loss and decrease of permeability across the here investigated stress range ±30 MPa. In this work, we have measured the stress dependence of the quasi-static and dynamic loss properties of high-purity 0.50 mm-thick NO Fe–(2 wt%)Si steel sheets and discussed the resulting monotonical increase of the loss at all frequencies following the passage from tensile to compressive stress. The main conclusions can be summarized as follows.

1) With an assumed distribution of the populated easy axes in compressed sheets and its evolution with the applied field, the magnetoelastic energy variation across the major hysteresis loop and its share compared to the magnetostatic energy is calculated. Recourse is made to the median curve, which identifies the reactive exchange of energy with the supply system. In this way, the frictional field H_f, fully associated with dissipation, is separated and a peculiar bulged appearance of the (H_f, J) curve in the second quadrant is singled out and justified. At 30 MPa compressive stress, H_f is estimated to be around 30 A/m, versus a coercive field in the unstressed state of 45 A/m.
2) The measurements performed up to $f = 400$ Hz and the loss separation procedure demonstrate the direct relationship existing between the quasi-static $W_{\rm hyst}$ and the dynamic excess loss $W_{\rm exc}$ components. $W_{\rm hyst}$ and $W_{\rm exc}$ exhibit parallel trends with the evolution of σ in sign and value, fulfilling the prediction of the STL.

We therefore find, for example, that the 20% increase to the measured loss at 50 Hz and $J_p = 1.5$ T introduced by a 30 MPa compressive stress is the result of 28% and 34% enhanced W_{hyst} and W_{exc} values (W_{class} is independent of σ).

3) The increase of permeability engendered by the tensile stress (Fig. 6) and its effect on incomplete flux penetration (skin effect) on approaching the upper frequency limit is dealt with by analytical calculation. In particular, the classical loss $W_{\text{class}}(f)$ is obtained by solution of Maxwell's diffusion equation. The involved magnetic constitutive equation of the material is approximated by the elliptical hysteresis loop having the same area and J_p values of the experimental dc loop. $W_{\text{class}}(f)$ is in this way expressed in terms of equivalent real and imaginary permeabilities. It becomes a non-linear function of frequency, with the slope declining toward $f^{1/2}$. At the same time, W_{hyst} is affected by the concurrent rise of non-uniform profile of the magnetization across the sheet thickness and is consequently found to slightly increase with the frequency.

ACKNOWLEDGMENT

This work was supported in part by the Fondo Italiano Scienze Applicate through the Materials and Design for Electric Engines under Project FISA-2022-00261. *(Enzo Ferrara, Olivier de la Barrière, Daniele Carosi, Alessandro Morri, Alessandro Ferraiuolo, and Fausto Fiorillo contributed equally to this work.)*

REFERENCES

[1] H. Hiwaki, H. Murakami, Y. Honda, M. Sanada, S. Morimoto, and Y. Takeda, "Reducing iron loss by decreasing stress in stator core of permanent magnet synchronous motor," *IEEJ Trans. Ind. Appl.*, vol. 126, no. 7, pp. 852–856, 2006, doi: 10.1541/ieejias.126.852.

[2] D. Miyagi, N. Maeda, Y. Ozeki, K. Miki, and N. Takahashi, "Estimation of iron loss in motor core with shrink fitting using FEM analysis," *IEEE Trans. Magn.*, vol. 45, no. 3, pp. 1704–1707, Mar. 2009, doi: 10.1109/TMAG.2009.2012790.

[3] D. Li, Y. Zhang, Y. Jing, D. Xie, and C.-S. Koh, "Core loss and deformation computation in permanent magnet linear motors considering the effect of stress on magnetic and magnetostrictive properties," in *Proc. 13th Int. Symp. Linear Drives Ind. Appl. (LDIA)*, Wuhan, China, Jul. 2021, pp. 1–5, doi: 10.1109/LDIA49489.2021.9505715.

[4] Y. Oda, H. Toda, N. Shiga, S. Kasai, and T. Hiratani, "Effect of Si content on iron loss of electrical steel sheet under compressive stress," *IEEE Trans. Magn.*, vol. 50, no. 4, pp. 1–4, Apr. 2014, doi: 10.1109/TMAG.2013.2290321.

[5] M. LoBue, C. Sasso, V. Basso, F. Fiorillo, and G. Bertotti, "Power losses and magnetization process in Fe–Si non-oriented steels under tensile and compressive stress," *J. Magn. Magn. Mater.*, vols. 215–216, pp. 124–126, Jun. 2000, doi: 10.1016/s0304-8853(00)00092-5.

[6] O. Perevertov, "Influence of the applied tensile and compressive stress on the hysteresis curves of Fe-3%Si non-oriented steel," *J. Magn. Magn. Mater.*, vol. 428, pp. 223–228, Apr. 2017, doi: 10.1016/j.jmmm.2016.12.040.

[7] V. Permiakov, L. Dupré, A. Pulnikov, and J. Melkebeek, "Loss separation and parameters for hysteresis modelling under compressive and tensile stresses," *J. Magn. Magn. Mater.*, vols. 272–276, pp. E553–E554, May 2004, doi: 10.1016/j.jmmm.2003.11.381.

[8] N. Leuning, S. Steentjes, M. Schulte, W. Bleck, and K. Hameyer, "Effect of elastic and plastic tensile mechanical loading on the magnetic properties of NGO electrical steel," *J. Magn. Magn. Mater.*, vol. 417, pp. 42–48, Nov. 2016, doi: 10.1016/j.jmmm.2016.05.049.

[9] A. P. S. Baghel, J. B. Blumenfeld, L. Santandrea, G. Krebs, and L. Daniel, "Effect of mechanical stress on different core loss components along orthogonal directions in electrical steels," *Electr. Eng.*, vol. 101, pp. 845–853, Aug. 2019, doi: 10.1007/s00202-019-00827-4.

[10] Y. Dou, Y. Li, C. Zhang, S. Yue, and J. Zhu, "Effects of uniaxial stress along different directions on alternating magnetic properties of silicon steel sheets," *IEEE Trans. Magn.*, vol. 56, no. 3, pp. 1–4, Mar. 2020, doi: 10.1109/TMAG.2019.2954465.

[11] M. J. Sablik and D. C. Jiles, "Coupled magnetoelastic theory of magnetic and magnetostrictive hysteresis," *IEEE Trans. Magn.*, vol. 29, no. 4, pp. 2113-2123, Jul. 1993, doi: 10.1109/20.221036.

[12] M. J. Sablik, "A model for asymmetry in magnetic property behavior under tensile and compressive stress in steel," *IEEE Trans. Magn.*, vol. 33, no. 5, pp. 3958–3960, May 1997, doi: 10.1109/20.619628.

[13] P. Rasilo et al., "Modeling of hysteresis losses in ferromagnetic laminations under mechanical stress," *IEEE Trans. Magn.*, vol. 52, no. 3, pp. 1–4, Mar. 2016, doi: 10.1109/TMAG.2015.2468599.

[14] C. S. Schneider, "Effect of stress on the shape of ferromagnetic hysteresis loops," *J. Appl. Phys.*, vol. 97, no. 10, May 2005, Art. no. 10E503, doi: 10.1063/1.1846451.

[15] D. Singh, P. Rasilo, F. Martin, A. Belahcen, and A. Arkkio, "Effect of mechanical stress on excess loss of electrical steel sheets," *IEEE Trans. Magn.*, vol. 51, no. 11, pp. 1–4, Nov. 2015, doi: 10.1109/TMAG.2015.2449779.

[16] A. P. S. Baghel, B. S. Ram, L. Daniel, S. V. Kulkarni, G. Krebs, and J. B. Blumenfeld, "An alternative approach to model mechanical stress effects on magnetic hysteresis in electrical steels using complex permeability," *Comp. Mater. Sci.*, vol. 166, pp. 96–104, Aug. 2019, doi: 10.1016/j.commatsci.2019.03.048.

[17] G. Bertotti, "General properties of power losses in soft ferromagnetic materials," *IEEE Trans. Magn.*, vol. MAG-24, no. 1, pp. 621–630, Jan. 1988, doi: 10.1109/20.43994.

[18] A. J. Schwartz, M. Kumar, B. L. Adams, and D. P. Field, *Electron Backscatter Diffraction in Materials Science*. Boston, MA, USA: Springer, 2009, doi: 10.1007/978-0-387-88136-2.

[19] F. J. Humphreys and M. Hatherly, *Recrystallization and Related Annealing Phenomena*, 2nd ed., Boston, MA, USA: Elsevier, 2004.

[20] C. Appino et al., "International comparison on SST and Epstein measurements in grain-oriented Fe-Si sheet steel," *Int. J. Appl. Electromagn. Mech.*, vol. 48, no. 2,3, pp. 123–133, Jun. 2015.

[21] F. Fiorillo, *Measurement and Characterization of Magnetic Materials*. New York, NY, USA: Academic, 2004, p. 340.

[22] D. Miyagi, K. Miki, M. Nakano, and N. Takahashi, "Influence of compressive stress on magnetic properties of laminated electrical steel sheets," *IEEE Trans. Magn.*, vol. 46, no. 2, pp. 318–321, Feb. 2010, doi: 10.1109/TMAG.2009.2033550.

[23] F. Fiorillo, M. Küpferling, and C. Appino, "Magnetic hysteresis and Barkausen noise in plastically deformed steel sheets," *Metals*, vol. 8, no. 1, p. 15, Dec. 2017, doi: 10.3390/met8010015.

[24] G. Bertotti, *Hysteresis in Magnetism*. New York, NY, USA: Academic, 1998, p. 391.

[25] L. R. Dupre, O. Bottauscio, M. Chiampi, M. Repetto, and J. A. A. Melkebeek, "Modeling of electromagnetic phenomena in soft magnetic materials under unidirectional time periodic flux excitations," *IEEE Trans. Magn.*, vol. 35, no. 5, pp. 4171–4184, May 1999, doi: 10.1109/20.799065.

[26] H. Zhao, C. Ragusa, O. de la Barrière, M. Khan, C. Appino, and F. Fiorillo, "Magnetic loss versus frequency in non-oriented steel sheets and its prediction: Minor loops, PWM, and the limits of the analytical approach," *IEEE Trans. Magn.*, vol. 53, no. 11, pp. 1–4, Nov. 2017, doi: 10.1109/TMAG.2017.2701299.

[27] H. Zhao, C. Ragusa, C. Appino, O. de la Barrière, Y. Wang, and F. Fiorillo, "Energy losses in soft magnetic materials under symmetric and asymmetric induction waveforms," *IEEE Trans. Power Electron.*, vol. 34, no. 3, pp. 2655–2665, Mar. 2019, doi: 10.1109/TPEL.2018.2837657.

[28] C. Beatrice, C. Appino, O. de la Barrière, F. Fiorillo, and C. Ragusa, "Broadband magnetic losses in Fe-Si and Fe-Co laminations," *IEEE Trans. Magn.*, vol. 50, no. 4, pp. 1–4, Apr. 2014, doi: 10.1109/TMAG.2013.2286923.

[29] G. Bertotti, "Direct relation between hysteresis and dynamic losses in soft magnetic materials," *J. Phys.*, vol. 46, no. C6, pp. 389–392, 1985, doi: 10.1051/jphyscol:1985672.

Carlo Appino received the M.Sc. degree in physics from the Università di Torino, Turin, Italy, in 1985, and the Ph.D. degree in physics from the Politecnico di Torino, Turin, in 1992.

He was an Invited Researcher at the MADEA Laboratory, CNRS, Grenoble, France, and the SATIE Laboratory, École Normale Supérieure, Cachan, France. He has been a Research Scientist at the Istituto Nazionale di Ricerca Metrologica (INRIM) (formerly Istituto Elettrotecnico Nazionale Galileo Ferraris), Turin, since 1994. His research activity has been mainly devoted to theoretical and experimental investigation of soft magnets, with particular reference to hysteresis phenomena and vector magnetization process.

Dr. Appino has been a member of the Steering Committee of the International Workshop on 1&2 Dimensional Magnetic Measurement and Testing since 2016 and the International Organizing Committee of the Conference Soft Magnetic Materials since 2017.

Enzo Ferrara is a Research Scientist at the Istituto Nazionale di Ricerca Metrologica (INRIM), Turin, Italy. He is involved in the maintenance and development of instrumental setup for magnetic measurements, and the elaboration and characterization of innovative, amorphous, micro- and nano-sized magnetic materials applied as core components in devices of electrotechnics.

Olivier de la Barrière received the M.S. and Ph.D. degrees in electrical engineering from the Ecole Normale Supérieure de Cachan, Cachan, France, in 2007 and 2010, respectively.

He was a Post-Doctoral Scientist at the National Institute of Research in Metrology, Turin, Italy. Since 2013, he has been a Full-Time Centre National de la Recherche Scientifique Researcher at the Systems and Applications of Information Technologies and Energy Laboratory (UMR8029), Gif-sur-Yvette, France. He is the co-author of 50 publications. His research interests include electrical machine design, axial flux machines, and iron loss measurement and modeling in soft magnets (laminated or granular).

Dr. de la Barrière has been a member of the International Electrotechnical Committee (IEC) for Standardization of Magnetic Measurements (TC68) since 2016.

Daniele Carosi received the master's degree in mechanical engineering from the University of Bologna, Bologna, Italy, in 2022, where he is currently pursuing the Ph.D. degree with the Aerospace Science and Technology Ph.D. School.

His research activities focus on identifying methodologies to derive simulation parameters for the equations related to the hysteresis loop simulations, the impact that the microstructural features of a metallic material have on its magnetization, and how to incorporate them into the simulation parameters.

Alessandro Morri is an Assistant Professor of metallurgy at the Department of Industrial Engineering, University of Bologna, Bologna, Italy. He has authored/co-authored about 100 peer-reviewed publications in national and international scientific journals. He coordinated international, national, and regional research projects concerning the metallurgy of light alloys, sintered steels, and soft magnetic materials. His research focuses on the relationships between the manufacturing process, microstructure, and metals' physical, chemical, and mechanical properties.

Alessandro Ferraiuolo received the degree in physics.

He was a Researcher of aeronautical composite materials at Finmeccanica (Leonardo SpA), Rome, Italy, in 1992. In 1994, he joined the Centro Sviluppo Materiali, Rome, as a Metallurgist. In 2012, he patented the first stainless twinning induced plasticity (TWIP) steel based on low Ni and high Cu–N–Mn composition. In 2015, he joined Marcegaglia Ravenna Steel Company, Ravenna, Italy, as an R&D Manager. In 2018, he developed a new theoretical approach to evaluate the work hardening in hot rolling opening the opportunity to adopt incremental plasticity theory. In 2019, he developed a zero CO_2 emission cold complex metallurgical cycle for non-oriented (NO) fully processed electrical steel production at the Marcegaglia Ravenna plant.

Fausto Fiorillo received the Laurea degree from the University of Torino, Turin, Italy, in 1972.

He started his career as a Physicist at the Istituto Nazionale di Ricerca Metrologica (INRIM) (formerly Istituto Elettrotecnico Nazionale Galileo Ferraris), Turin, in 1974. He has been the Research Director of INRIM since 2012, where he is the Emeritus Scientist. He has authored/co-authored some 230 peer-reviewed publications in international scientific journals, review monographs, and chapters on international series on magnetic materials. He is the author of the comprehensive treatise *Measurement and Characterization of Magnetic Materials* (Academic Press-Elsevier, 2004). His scientific work and research interests include the properties of magnetic materials and their measurement.

Open Access funding provided by 'Istituto Nazionale di Ricerca Metrologica - INRiM' within the CRUI CARE Agreement